POLARIZATION CHARACTERISTICS OF THE COHERENT BACKSCATTER OPPOSITION EFFECT

M. I. MISHCHENKO*

The Main Astronomical Observatory of the Ukrainian Academy of Sciences, Goloseevo, Kiev, Ukraine

(Received 7 February 1992)

Abstract. It has been suggested recently that coherent backscattering of photons from discrete disordered media, which has been recently discovered in laboratory-controlled experiments, may play a role in peculiar radar and light scattering from some atmosphereless solar system bodies. In this paper, a rigorous vector theory recently developed by Mishchenko (1991b, 1992a) is used to study polarization characteristics of the coherent backscatter opposition effect. Backscattering enhancement in different polarization components is studied and results of computer calculations for a representative selection of scattering models are presented. It is pointed out that these calculations support recent Hapke's (1990) explanation of unusual radar characteristics of icy outer planet satellites.

1. Introduction

It has been suggested recently that weak localization of photons in (or coherent backscattering from) discrete disordered media can account for peculiar reflectance properties of some atmosphereless solar system bodies. Hapke (1990) has suggested that unusual radar reflectivity of icy outer planet satellites may be explained by weak localization of centimeter radiowaves in a regolith consisting of voids and/or silicate rocks in an icy matrix and has pointed out that if multiple scattering among macroscopic particles of Saturn's rings is important in their radar reflectivity, then coherent backscattering should also occur there. Mishchenko and Dlugach (1992a) and Mishchenko (1992b) have suggested that unusually narrow opposition effect of some icy satellites and Saturn's rings at visible and near infrared wavelengths may be explained by coherent backscattering of light from upper, optically active layers of submicrometer-sized regolithic grains composed of water ice.

For media composed of randomly distributed scattering particles and illuminated by a parallel beam of light, weak localization manifests itself as a well-defined narrow peak centered at zero phase angle, which is observed in the reflected light for both intensity and polarization (see, e.g., Sheng, 1990; Nieto-Vesperinas and Dainty, 1990). The scalar theory of weak localization is now basically well understood (e.g., Akkermans *et al.*, 1988; Barabanenkov and Ozrin, 1988; Ishimaru and Tsang, 1988; van der Mark *et al.*, 1988). According to this theory, the multiply scattered radiation reflected by discrete random media is composed of two parts. The first part is the diffusely scattered background radiation, which comes from the sum of the so-called ladder terms of the Bethe–Salpeter equation. The second

* *Address for correspondence:* NASA/GISS, 2880 Broadway, New York, NY 10025, U.S.A.

Earth, Moon, and Planets **58**: 127–144, 1992.

part is the coherent backscattering peak, which arises because a wave scattered through a certain multiple-scattering path can interfere with the wave scattered through the time-reversed path (i.e., the path that involves the same scatterers but in the reversed order), the interference being constructive in the backscattering direction. This coherent part of the reflected radiation comes from the sum of the so-called cyclical terms of the Bethe–Salpeter equation (for terminology, see, e.g., Frisch, 1968; and Tsang *et al.*, 1985).

Though the scalar theory is developed in detail, qualitatively explains the interference nature of weak localization, and quantitatively correctly predicts the angular width of the coherent backscattering peak, it cannot explain polarization effects that are observed in laboratory-controlled experiments. In particular, the scalar theory cannot reproduce the amplitudes of the backscattering peaks that are observed in the cross-polarization for linearly polarized incident light (e.g., Wolf *et al.*, 1988; van Albada *et al.*, 1988) and in the opposite-helicity channel for circularly polarized incident light (e.g., Etemad *et al.*, 1987). Furthermore, the scalar theory fails to predict quantitatively the amplitude of the coherent opposition effect observed in the intensity for unpolarized incident light (Mishchenko, 1992a; Mishchenko and Dlugach, 1992b). On the other hand, accurate numerical computations of these amplitudes for a representative selection of scattering models would be of importance for better understanding of the vector nature of weak localization and for many astrophysical applications (e.g., Hapke, 1990). Therefore, it is the aim of this paper to provide others with a compendium of such computations. To this end, we use a rigorous vector theory that has been recently developed by Mishchenko (1991b, 1992a). This theory enables one to perform accurate vector calculations of the coherent backscattering at exactly the backscattering direction (i.e., at zero phase angle) for rather realistic scattering models and was found to be in good agreement with results of laboratory-controlled experiments.

The paper is organized as follows. In Section 2, basic polarimetric definitions are briefly recapitulated and backscattering enhancement factors and polarization ratios for different representations of polarization are introduced. In Section 3, general properties of the backscattering enhancement factors are studied. In Section 4, results of computer calculations for a representative selection of scattering models are presented and dependence of the enhancement factors and polarization ratios on the properties of the medium is studied. Finally, in Section 5, the results of the paper are summarized and discussed.

2. Basic Definitions and Formulae

We model the scattering medium by a locally plane-parallel slab composed of

randomly distributed, independently scattering particles.* For simplicity, we assume that the scattering medium is macroscopically isotropic. This implies that the scattering particles are randomly oriented and (i) each particle has a plane of symmetry and/or (ii) particles and their mirror particles are present in equal numbers (van de Hulst, 1957). The direction of light incident on or reflected by the slab is specified by the polar angle $0 \leqslant \theta \leqslant \pi$, which is measured from the inward normal to the upper boundary of the slab, and by the azimuth angle $0 \leqslant \varphi \leqslant 2\pi$.

To describe the state of polarization of a beam of light, we use three familiar representations of polarization, namely, the coherency (or density) matrix representation **D**, the Stoke vector representation **I**, and the circular-polarization representation $\mathbf{I}_{\mathrm{CP}}$ (e.g., Hovenier and van der Mee, 1983; Ishimaru and Yeh, 1984). These four-component vectors are defined as

$$\mathbf{D} = \begin{bmatrix} E_\theta E_\theta^* \\ E_\theta E_\varphi^* \\ E_\varphi E_\theta^* \\ E_\varphi E_\varphi^* \end{bmatrix}, \tag{2.1}$$

$$\mathbf{I} = \begin{bmatrix} I \\ Q \\ U \\ V \end{bmatrix} = \begin{bmatrix} D_1 + D_4 \\ D_1 - D_4 \\ -iD_2 - iD_3 \\ -iD_2 + iD_3 \end{bmatrix}, \tag{2.2}$$

$$I_{\mathrm{CP}} = \frac{1}{2} \begin{bmatrix} Q + iU \\ I + V \\ I - V \\ Q - iU \end{bmatrix}, \tag{2.3}$$

where E_θ and E_φ are the θ- and φ-components of the electric vector, and the asterisk denotes the conjugate complex value.

Let the slab be illuminated by a parallel beam of light incident in the direction $(\theta_0, \varphi_0 = 0)$ and let **S** be the Stokes reflection matrix for exactly the backscattering direction $(\pi - \theta_0, \pi)$. The matrix **S** of the block-diagonal form

* Note that in regolithic layers, the particles are, most likely, densely packed rather than sparsely distributed. Therefore, the assumption of independent scattering may seem to be unrealistic. However, this assumption greatly simplifies theoretical considerations and was shown by Mishchenko (1991b) to give good results even for rather densely packed media.

$$\mathbf{S} = \begin{bmatrix} S_{11} & S_{12} & 0 & 0 \\ S_{12} & S_{22} & 0 & 0 \\ 0 & 0 & S_{33} & S_{34} \\ 0 & 0 & -S_{34} & S_{44} \end{bmatrix}, \tag{2.4}$$

transforms the Stokes vector of the incident light $\mathbf{I}^0$ into the Stokes vector of the reflected light $\mathbf{I}$:

$$\mathbf{I} = \frac{\cos\theta_0 \mathbf{S}\mathbf{I}^0}{\pi}. \tag{2.5}$$

In accordance with the theory of weak localization, the matrix $\mathbf{S}$ may be decomposed as

$$\mathbf{S} = \mathbf{S}^1 + \mathbf{S}^L + \mathbf{S}^C = \mathbf{S}^D + \mathbf{S}^C, \qquad \mathbf{S}^D = \mathbf{S}^1 + \mathbf{S}^L, \tag{2.6}$$

where $\mathbf{S}^1$ is the contribution of the first-order scattering, $\mathbf{S}^L$ is the contribution of all the ladder diagrams of orders $n \geqslant 2$, and $\mathbf{S}^C$ is the contribution of all the cyclical diagrams. The diffusely scattered, background component comes from the sum $\mathbf{S}^D = \mathbf{S}^1 + \mathbf{S}^L$, while the coherent opposition peak comes from the cyclical contribution $\mathbf{S}^C$. For media composed of spherical or randomly oriented nonspherical particles, the matrices $\mathbf{S}^1$ and $\mathbf{S}^D$ (or $\mathbf{S}^L$) may be found by solving Chandrasekhar's vector radiative transfer equation (see, e.g., Hansen and Travis, 1974; de Rooij, 1985; de Haan *et al.*, 1987; Mishchenko, 1990, 1991a). After calculating the matrix $\mathbf{S}^L$, the matrix $\mathbf{S}^C$ may be found from the relation (Mishchenko, 1992a)

$$\mathbf{S}^C = \begin{bmatrix} S_{11}^C & S_{12}^L & 0 & 0 \\ S_{12}^L & S_{22}^C & 0 & 0 \\ 0 & 0 & S_{33}^C & S_{34}^L \\ 0 & 0 & -S_{34}^L & S_{44}^C \end{bmatrix}, \tag{2.7}$$

where

$$S_{11}^C = \tfrac{1}{2}(S_{11}^L + S_{22}^L - S_{33}^L + S_{44}^L), \tag{2.8a}$$

$$S_{22}^C = \tfrac{1}{2}(S_{11}^L + S_{22}^L + S_{33}^L - S_{44}^L), \tag{2.8b}$$

$$S_{33}^C = \tfrac{1}{2}(-S_{11}^L + S_{22}^L + S_{33}^L + S_{44}^L), \tag{2.8c}$$

$$S_{44}^C = \tfrac{1}{2}(S_{11}^L - S_{22}^L + S_{33}^L + S_{44}^L). \tag{2.8d}$$

In the coherency matrix and circular-polarization representations, we have, respectively (Mishchenko, 1991b, 1992a)

$$\mathbf{G}^{\mathrm{C}} = \begin{bmatrix} G_{11}^{\mathrm{L}} & 0 & 0 & -G_{23}^{\mathrm{L}} \\ 0 & G_{22}^{\mathrm{L}} & -G_{14}^{\mathrm{L}} & 0 \\ 0 & -G_{14}^{\mathrm{L}} & G_{33}^{\mathrm{L}} & 0 \\ -G_{23}^{\mathrm{L}} & 0 & 0 & G_{44}^{\mathrm{L}} \end{bmatrix}, \tag{2.9}$$

$$\mathbf{C}^{\mathrm{C}} = \begin{bmatrix} C_{11}^{\mathrm{L}} & C_{12}^{\mathrm{L}} & C_{12}^{\mathrm{L}*} & C_{23}^{\mathrm{L}} \\ C_{12}^{\mathrm{L}} & C_{22}^{\mathrm{L}} & C_{14}^{\mathrm{L}} & C_{12}^{\mathrm{L}*} \\ C_{12}^{\mathrm{L}*} & C_{14}^{\mathrm{L}} & C_{22}^{\mathrm{L}} & C_{12}^{\mathrm{L}} \\ C_{23}^{\mathrm{L}} & C_{12}^{\mathrm{L}*} & C_{12}^{\mathrm{L}} & C_{11}^{\mathrm{L}} \end{bmatrix}, \tag{2.10}$$

where $\mathbf{G}$ and $\mathbf{C}$ are the corresponding backscattering matrices of the form

$$\mathbf{G} = \begin{bmatrix} G_{11} & 0 & 0 & G_{14} \\ 0 & G_{22} & G_{23} & 0 \\ 0 & G_{23} & G_{33} & 0 \\ G_{14} & 0 & 0 & G_{44} \end{bmatrix}, \tag{2.11}$$

and

$$\mathbf{C} = \begin{bmatrix} C_{11} & C_{12} & C_{12}^{*} & C_{14} \\ C_{12} & C_{22} & C_{23} & C_{12}^{*} \\ C_{12}^{*} & C_{23} & C_{22} & C_{12} \\ C_{14} & C_{12}^{*} & C_{12} & C_{11} \end{bmatrix}. \tag{2.12}$$

Equations (2.1)–(2.12) may be used to define several backscattering enhancement factors that correspond to particular experimental or natural conditions.

(i) For unpolarized incident light with $\mathbf{I}^0 = (1, 0, 0, 0)^T$, the intensity backscattering enhancement factor ζ_I is defined as the ratio of the total backscattered intensity to the incoherent background intensity:

$$\zeta_I = \frac{S_{11}^1 + S_{11}^L + S_{11}^{\mathrm{C}}}{S_{11}^1 + S_{11}^{\mathrm{L}}}. \tag{2.13}$$

Also, we define the intensity of the incoherent background as

$$I = \frac{(S_{11}^1 + S_{11}^{\mathrm{L}}) \cos \theta_0}{\pi}. \tag{2.14}$$

(ii) For linearly polarized incident light with electric vector in the meridional plane (i.e., the plane through the beam and the normal to the boundaries of the

slab), $\mathbf{D}^0 = (1, 0, 0, 0)^T$, the copolarized backscattering enhancement factor $\zeta_\parallel^1$ is defined as the ratio of the total to incoherent intensity in the copolarized channel:

$$\zeta_\parallel^1 = \frac{G_{11}^1 + G_{11}^L + G_{11}^c}{G_{11}^1 + G_{11}^L}. \tag{2.15}$$

Similarly, the cross-polarized enhancement factor $\zeta_\perp$ is defined as the ratio of the total to diffuse intensity in the cross-polarized channel, i.e.,

$$\zeta_\perp = \frac{G_{14}^1 + G_{14}^L + G_{14}^C}{G_{14}^1 + G_{14}^L}. \tag{2.16}$$

For linearly polarized incident light with electric vector perpendicular to the meridional plane, $\mathbf{D}^0 = (0, 0, 0, 1)^T$, the copolarized backscattering enhancement factor $\zeta_\parallel^2$ is defined as

$$\zeta_\parallel^2 = \frac{G_{44}^1 + G_{44}^L + G_{44}^C}{G_{44}^1 + G_{44}^L}, \tag{2.17}$$

while the corresponding cross-polarized enhancement factor is given by Equation (2.16).

Also, we define the corresponding linear polarization ratios of the incoherent background, $\chi_L^{1,2}$, and of the backscattering peak, $\mu_L^{1,2}$, as ratios of the crosspolarized to copolarized intensities:

$$\chi_L^1 = \frac{G_{14}^1 + G_{14}^L}{G_{11}^1 + G_{11}^L}, \tag{2.18}$$

$$\chi_L^2 = \frac{G_{14}^1 + G_{14}^L}{G_{44}^1 + G_{44}^L}, \tag{2.19}$$

$$\mu_L^1 = \frac{G_{14}^1 + G_{14}^L + G_{14}^C}{G_{11}^1 + G_{11}^L + G_{11}^C}, \tag{2.20}$$

$$\mu_L^2 = \frac{G_{14}^1 + G_{14}^L + G_{14}^C}{G_{44}^1 + G_{44}^L + G_{44}^C}. \tag{2.21}$$

(iii) For circularly polarized incident light with $\mathbf{I}_{CP}^0 = (0, 1, 0, 0)^T$, we define the backscattering enhancement factors in the helicity-preserving channel, ζ_{hp}, and in the opposite-helicity channel, ζ_{oh}, as

$$\zeta_{hp} = \frac{C_{22}^1 + C_{22}^L + C_{22}^C}{C_{22}^1 + C_{22}^L}, \tag{2.22}$$

$$\zeta_{oh} = \frac{C_{23}^1 + C_{23}^L + C_{23}^C}{C_{23}^1 + C_{23}^L}. \tag{2.23}$$

Also, we define the circular polarization ratios of the incoherent background, χ_C,

and of the backscattering peak, μ_C, as ratios of the intensities in the helicity-preserving channel to the intensities in the opposite-helicity channel, i.e.,

$$\chi_C = \frac{C_{22}^{l} + C_{22}^{L}}{C_{23}^{l} + C_{23}^{L}}, \tag{2.24}$$

$$\mu_C = \frac{C_{22}^{l} + C_{22}^{L} + C_{22}^{C}}{C_{23}^{l} + C_{23}^{L} + C_{23}^{C}}. \tag{2.25}$$

3. General Properties of the Backscattering Enhancement Factors

For macroscopically isotropic media, the Stokes matrix $\mathbf{S}^1$ has the form (cf. van de Hulst, 1957; Bohren and Huffman, 1983)

$$\mathbf{S}^1 = \mathrm{diag}(S_{11}^1, S_{22}^1, S_{33}^1, S_{44}^1)\,. \tag{3.1}$$

For spherical particles,

$$S_{11}^1 = S_{22}^1 \quad \text{and} \quad S_{11}^1 = -S_{44}^1\,. \tag{3.2}$$

For randomly-oriented nonspherical particles, these equalities do not generally hold.

It is convenient to rewrite Equations (2.13), (2.15)–(2.17), (2.22), and (2.23) in terms of the matrices $\mathbf{S}^1$ and $\mathbf{S}^L$. We have

$$\zeta_I = \frac{S_{11}^1 + S_{11}^L + \frac{1}{2}(S_{11}^L + S_{22}^L - S_{33}^L + S_{44}^L)}{S_{11}^1 + S_{11}^L}, \tag{3.3}$$

$$\zeta_\parallel^1 = \frac{S_{11}^1 + S_{22}^1 + 2S_{11}^L + 4S_{12}^L + 2S_{22}^L}{S_{11}^1 + S_{22}^1 + S_{11}^L + 2S_{12}^L + S_{22}^L}, \tag{3.4}$$

$$\zeta_\parallel^2 = \frac{S_{11}^1 + S_{22}^1 + 2S_{11}^L - 4S_{12}^L + 2S_{22}^L}{S_{11}^1 + S_{22}^1 + S_{11}^L - 2S_{12}^L + S_{22}^L}, \tag{3.5}$$

$$\zeta_\perp = \frac{S_{11}^1 - S_{22}^1 + S_{11}^L - S_{22}^L - S_{33}^L + S_{44}^L}{S_{11}^1 - S_{22}^1 + S_{11}^L - S_{22}^L}, \tag{3.6}$$

$$\zeta_{hp} = \frac{S_{11}^1 + S_{44}^1 + 2S_{11}^L + 2S_{44}^L}{S_{11}^1 + S_{44}^1 + S_{11}^L + S_{44}^L}, \tag{3.7}$$

$$\zeta_{oh} = \frac{S_{11}^1 - S_{44}^1 + S_{11}^L + S_{22}^L - S_{33}^L - S_{44}^L}{S_{11}^1 - S_{44}^1 + S_{11}^L - S_{44}^L}. \tag{3.8}$$

The vector radiative transfer equation together with Equations (3.1)–(3.8) can be used to derive some general properties of the backscattering enhancement factors. For grazing incidence, small single-scattering albedos w, or small optical thicknesses of the slab τ, the main contribution to the backscattered incoherent

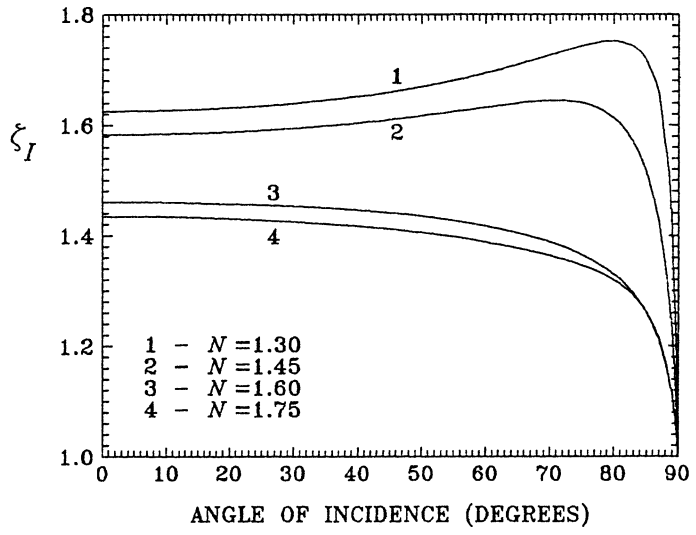

Fig. 1. The backscattering enhancement factor ζ_I versus the angle of incidence θ_0 for the semi-infinite homogeneous slab composed of polydisperse spherical particles with $a = \lambda$, $b = 0.05$, and $N = 1.3$, 1.45, 1.6, and 1.75.

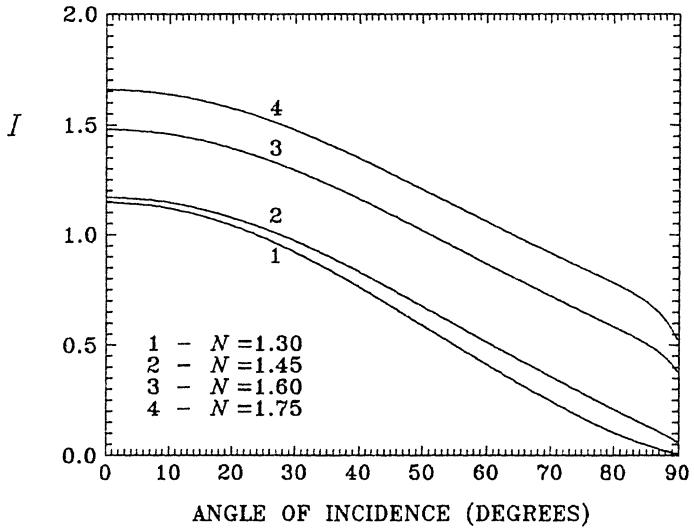

Fig. 2. As in Figure 1, for the intensity I.

background comes from the singly scattered photons. Therefore, one easily finds by inspection that the factors $\zeta_{\parallel}^{1,2}$, ζ_I, and ζ_{oh} obey the limits (Mishchenko, 1992a)

$$\lim_{\theta_0 \to \pi/2} \xi = \lim_{w \to 0} \xi = \lim_{\tau \to 0} \xi = 1 , \tag{3.9}$$

where ξ stands for $\zeta_{\parallel}^{1,2}$, ζ_I, or ζ_{oh}. For spherical particles, the factor $\zeta_{\perp}$ has no such definite limits, while

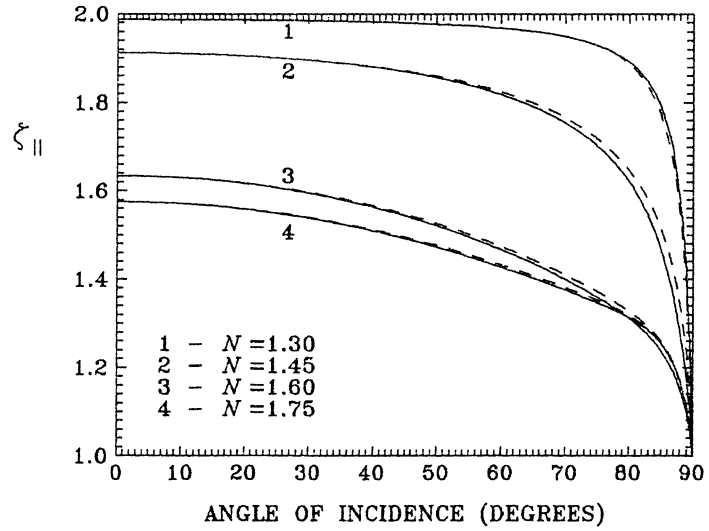

Fig. 3. As in Figure 1, for the factors $\zeta_{\|}^1$ (solid lines) and $\zeta_{\|}^2$ (dashed lines).

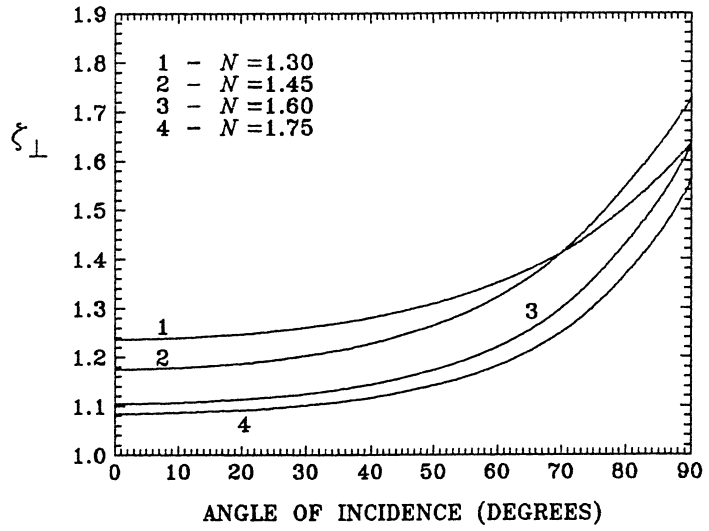

Fig. 4. As in Figure 1, for the factor $\zeta_{\perp}$.

$$\zeta_{\mathrm{hp}}|_{\mathrm{spheres}} \equiv 2\,. \tag{3.10}$$

For randomly-oriented nonspherical particles, the factors $\zeta_{\perp}$ and ζ_{hp} obey the limits of Equation (3.9). Also, for the case of normal incidence,

$$\zeta_{\|}^1(\theta_0 = 0) = \zeta_{\|}^2(\theta_0 = 0), \qquad \chi_{\mathrm{L}}^1(\theta_0 = 0) = \chi_{\mathrm{L}}^2(\theta_0 = 0),$$
$$\mu_{\mathrm{L}}^1(\theta_0 = 0) = \mu_{\mathrm{L}}^2(\theta_0 = 0) \tag{3.11}$$

(see Hovenier and de Haan, 1985).

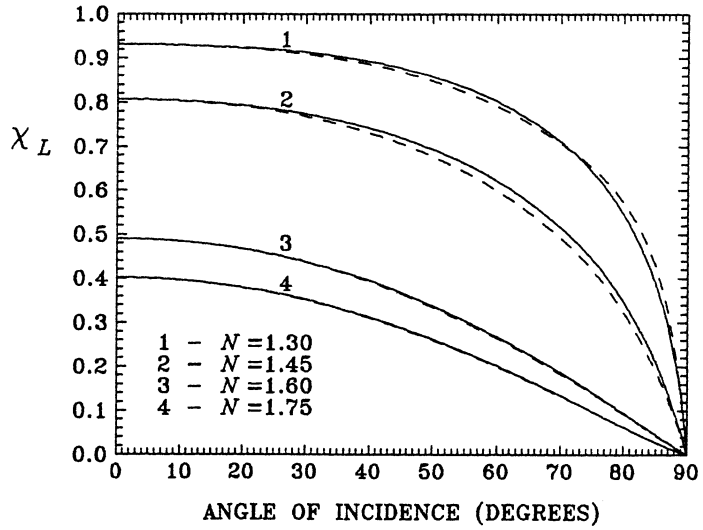

Fig. 5. As in Figure 1, for the polarization ratios χ_L^1 (solid lines) and χ_L^2 (dashed lines).

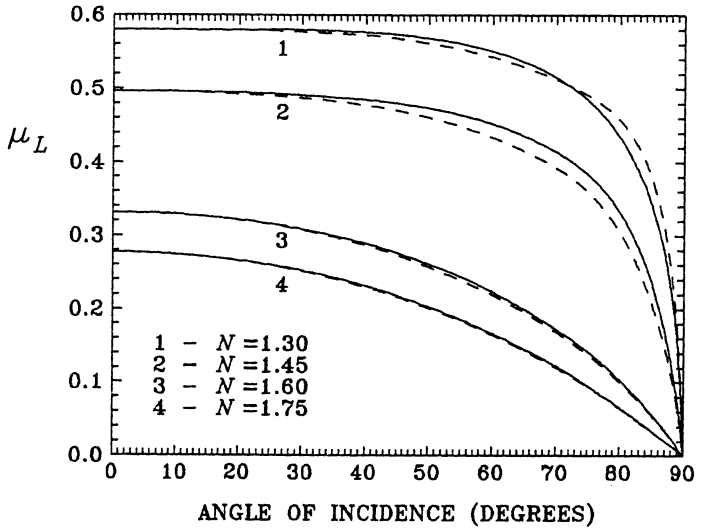

Fig. 6. As in Figure 1, for the polarization ratios μ_L^1 (solid lines) and μ_L^2 (dashed lines).

Additional properties of the backscattering enhancement factors can be derived by using the inequalities that must be satisfied by any Stokes transformation matrix of the block-diagonal form

$$\begin{bmatrix} a & b & 0 & 0 \\ b & c & 0 & 0 \\ 0 & 0 & d & e \\ 0 & 0 & -e & f \end{bmatrix},$$

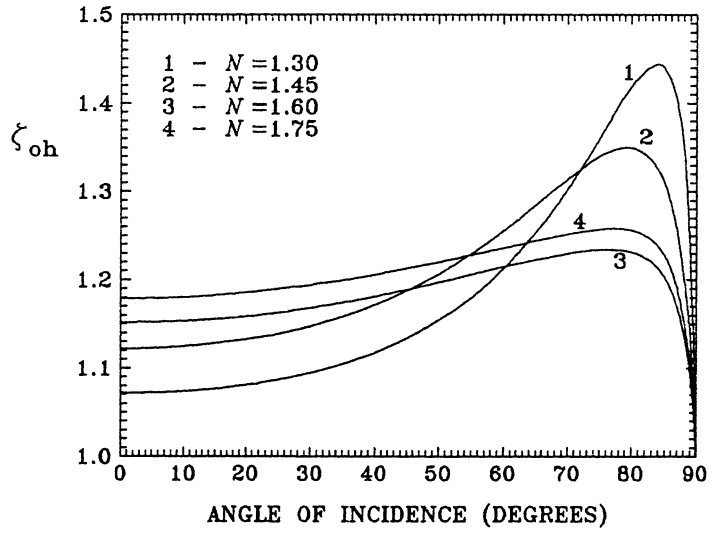

Fig. 7. As in Figure 1, for the factor ζ_{oh}.

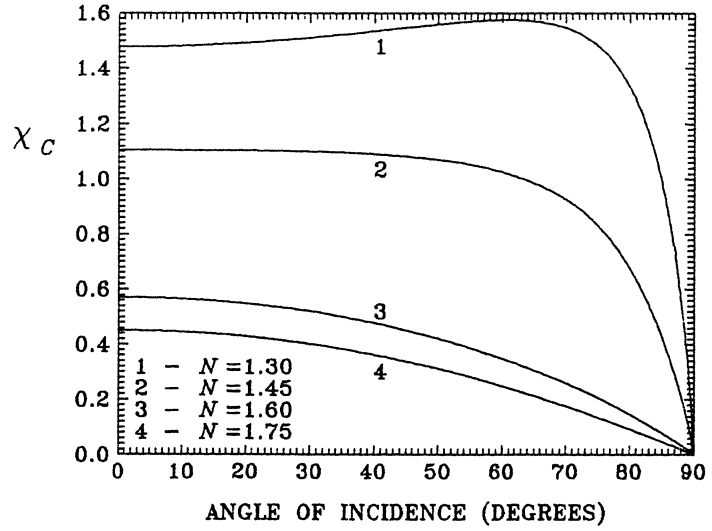

Fig. 8. As in Figure 1, for the polarization ratio χ_C.

(see Section 3.3 of Hovenier *et al.*, 1986). By applying these inequalities to the matrix $\mathbf{S}^L$, we have from Equations (3.3)–(3.8)

$$1 \leqslant \zeta_{\parallel}^{1,2} \leqslant 2\,, \tag{3.12}$$

$$0 \leqslant \zeta_{\perp} \leqslant 2\,, \tag{3.13}$$

$$0 \leqslant \zeta_{I} \leqslant 2\,, \tag{3.14}$$

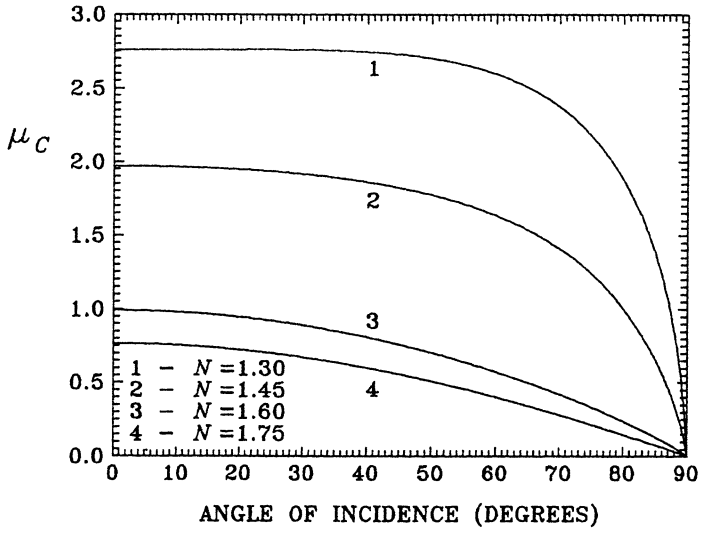

Fig. 9. As in Figure 1, for the polarization ratio μ_C.

$$1 \leqslant \zeta_{hp} \leqslant 2\,, \tag{3.15}$$

$$0 \leqslant \zeta_{oh} \leqslant 2\,. \tag{3.16}$$

4. Calculations and Discussion

In this section, we present results of numerical calculations for several scattering models. For simplicity, we assume that the scattering slab is homogeneous and optically thick (semi-infinite) and is composed of lossless spherical particles with radii governed by the standard gamma distribution (Hansen and Hovenier, 1974)

$$n(r) = \text{constant} \times r^{(1-3b)/b} \exp[-r/(ab)]\,, \tag{4.1}$$

where a is the effective radius and b is the effective variance. In all of our computations, the value $b = 0.05$ was used. To calculate the matrices $\mathbf{S}^1$ and $\mathbf{S}^L$ for the semi-infinite slab, we used de Rooij's (1985) numerical procedures.

In Figures 1–9, the computations are given for particles with $a/\lambda = 1$ and four values of the refractive index $N = 1.3$, 1.45, 1.6, and 1.75, where λ is the free-space wavelength. In Figures 10–18, the computations are reported for Rayleigh scattering (particle radii are much smaller than the wavelength) and spherical particles with $N = 1.45$ and three values of the effective radius $a = 0.3$, 1, and 2 μm. The wavelength is $\lambda = 1$ μm.

The following obvious properties of the backscattering enhancement factors and polarization ratios can be extracted from the numerical data shown.

(i) In the resonance region of particle radii ($a \sim \lambda$), the factor ζ_I is almost independent of a.

(ii) The factor ζ_I is a monotonically decreasing function of the angle of incidence

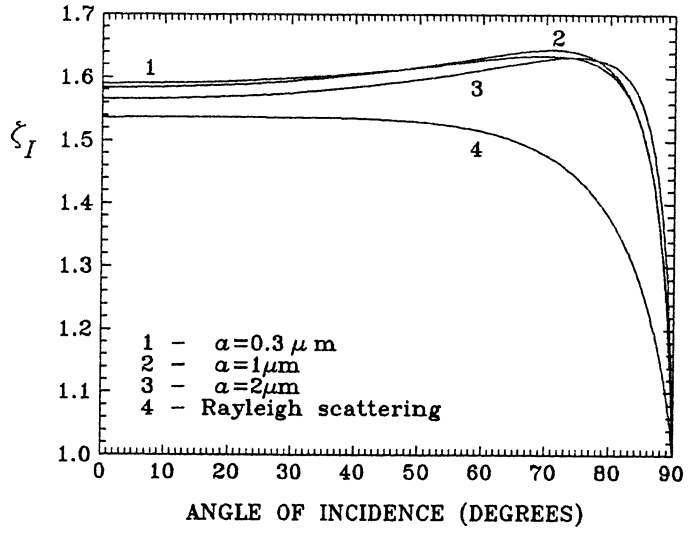

Fig. 10. The backscattering enhancement factor ζ_I versus the angle of incidence θ_0 for the semi-infinite homogeneous slab composed of polydisperse spherical particles with $N = 1.45$, $b = 0.05$, and $a = 0.3$, 1, and 2 μm and of particles much smaller than the wavelength (Rayleigh scattering). The wavelength is $\lambda = 1$ μm.

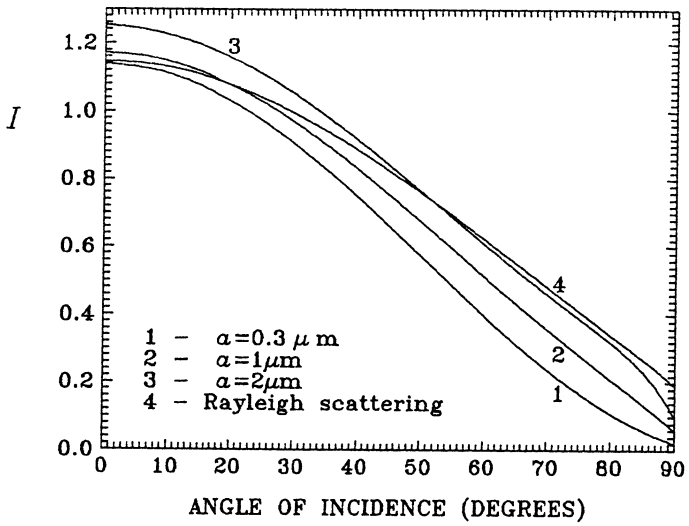

Fig. 11. As in Figure 10, for the intensity I.

for large refractive indices, while for small refractive indices it may have a maximum at $\theta_0 \neq 0$.

(iii) The factors $\zeta_{\parallel}^1$ and $\zeta_{\parallel}^2$ are always monotonically decreasing functions of the angle of incidence. The difference between these two factors is (very) small for Mie particles, but is substantial for Rayleigh scattering.

(iv) The factor ζ_I is usually smaller than the factors $\zeta_{\parallel}^{1,2}$.

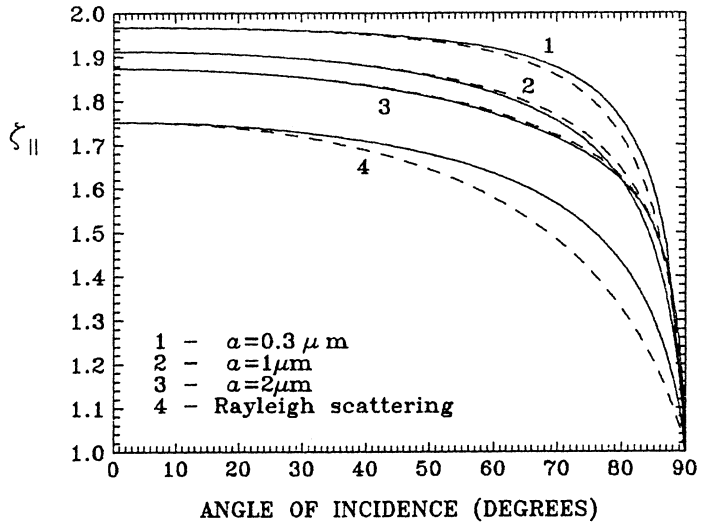

Fig. 12. As in Figure 10, for the factors $\zeta_{\|}^{1}$ (solid lines) and $\zeta_{\|}^{2}$ (dashed lines).

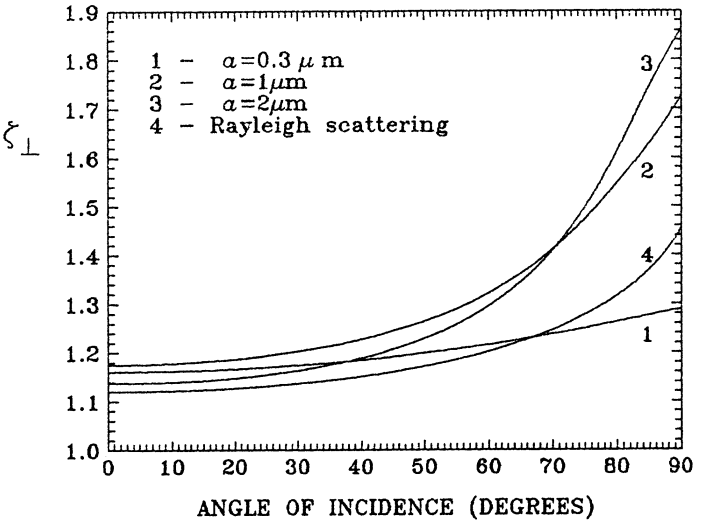

Fig. 13. As in Figure 10, for the factor $\zeta_{\perp}$.

(v) The factors ζ_{I} and $\zeta_{\|}^{1,2}$ are much smaller for larger refractive indices. This is a consequence of the increasing contribution of the first-order scattering.

(vi) The factor $\zeta_{\perp}$ is always a monotonically increasing function of the angle of incidence.

(vii) The factor $\zeta_{\perp}$ is (much) smaller than the factors $\zeta_{\|}^{1,2}$ at small angles of incidence, but may become larger at angles of incidence near 90°.

(viii) The factor ζ_{oh} is (much) smaller than the factor $\zeta_{\mathrm{hp}} \equiv 2$ (see Equation (3.10)).

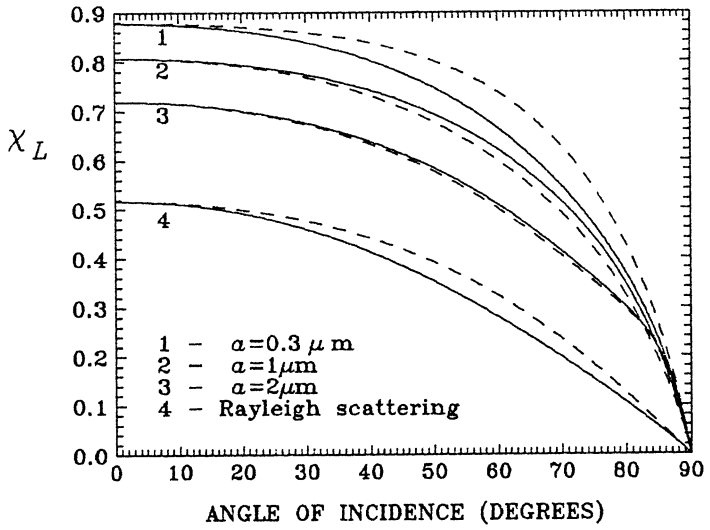

Fig. 14. As in Figure 10, for the polarization ratios χ_L^1 (solid lines) and χ_L^2 (dashed lines).

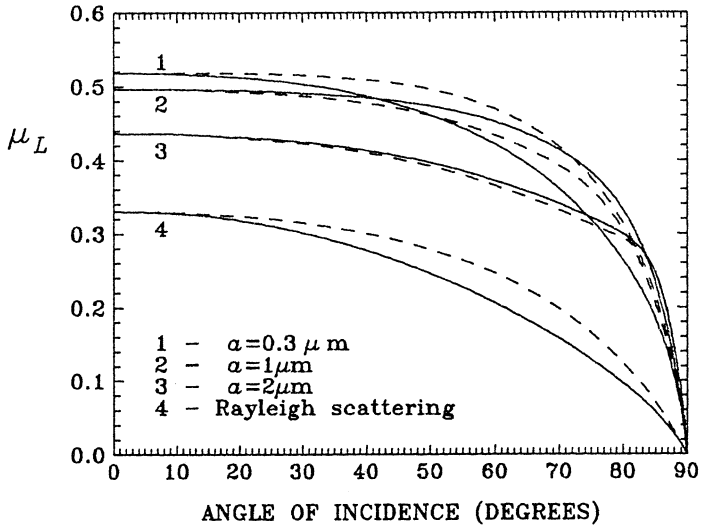

Fig. 15. As in Figure 10, for the polarization ratios μ_L^1 (solid lines) and μ_L^2 (dashed lines).

(ix) The factor ζ_{oh} has a (sharp) maximum at around $\theta_0 = 80°$.

(x) The linear and circular polarization ratios are smaller for larger refractive indices. This results from the increasing contribution of the first-order scattering.

5. Summary and Conclusions

In this paper, a rigorous vector theory of weak localization for exactly the backscattering direction was used to study how polarization characteristics of the

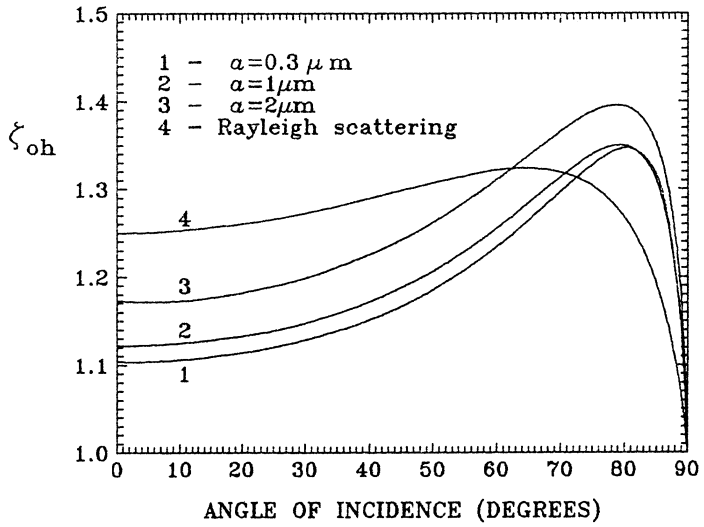

Fig. 16. As in Figure 10, for the factor ζ_{oh}.

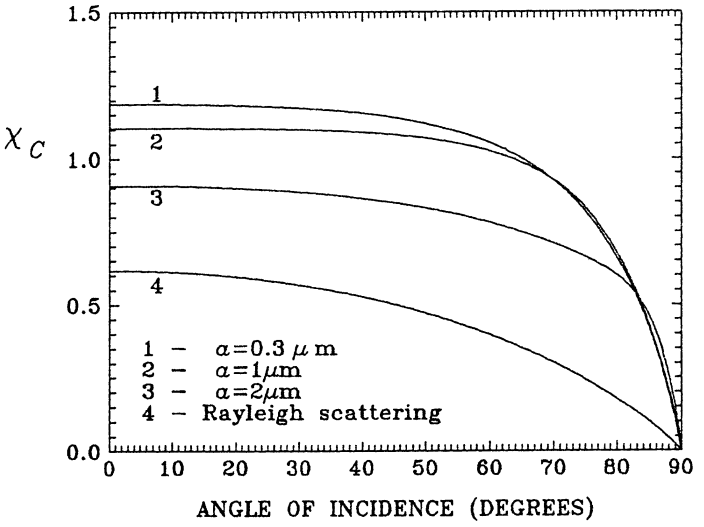

Fig. 17. As in Figure 10, for the polarization ratio χ_C.

coherent backscatter opposition effect depend on the properties of the scattering medium. We have presented a compendium of calculations for a representative selection of scattering models which, we hope, will be useful to those analysing observational data.

Although our aim here was not to use the theory for interpretation of some observations, it should be noted that our calculations support Hapke's recent explanation of unusual radar characteristics of icy outer planet satellites (Hapke, 1990). Radar observations of these satellites at centimeter wavelengths show that

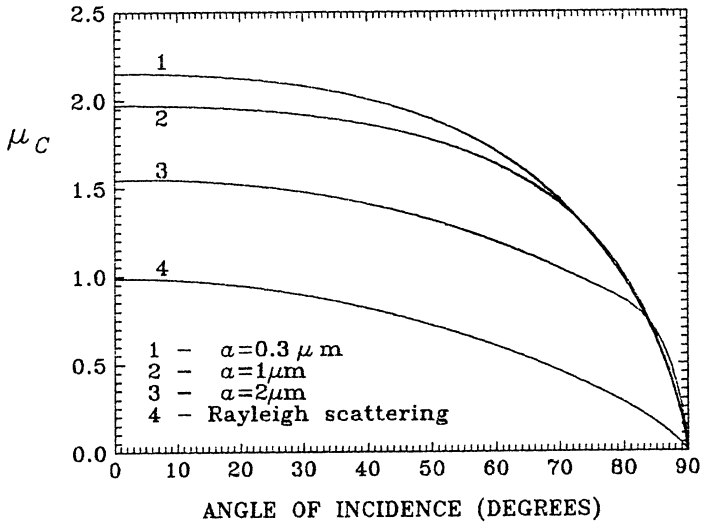

Fig. 18. As in Figure 10, for the polarization ratio μ_C.

when illuminated and observed in linearly polarized radiation, $\mu_I \approx 0.5$, while when illuminated and observed in circularly polarized radiation, $\mu_C > 1$ (e.g., Ostro, 1982). Our calculations show that multiple scattering and weak localization of radio waves in discrete disordered media can easily result in the observed values of these polarization ratios.

References

Akkermans, E., Wolf, P. E., Maynard, R., and Maret, G.: 1988, *J. Phys.* (*Paris*) **49**, 77.
Barabanenkov, Yu. N. and Ozrin, V. D.: 1988, *Zh. Eksper. Teor. Fiz.* **94**, 56.
Bohren, C. F. and Huffman, D. R.: 1983, *Absorption and Scattering of Light by Small Particles*, Wiley, New York.
de Haan, J. F., Bosma, P. B., and Hovenier, J. W.: 1987, *Astron. Astrophys.* **183**, 371.
de Rooij, W. A.: 1985, Ph.D. Thesis, Free University, Amsterdam.
Etemad, E., Thompson, R., Andrejco, M. J., John, S., and MacKintosh, F. C.: 1987, *Phys. Rev. Lett.* **59**, 1420.
Frisch, U.: 1968, in A. T. Bharucha-Reid (ed.), *Probabilistic Methods in Applied Mathematics*, Academic Press, New York, p. 75.
Hansen, J. E. and Hovenier, J. W.: 1974, *J. Atmos Sci.* **31**, 1137.
Hansen, J. E. and Travis, L. D.: 1974, *Space Sci. Rev.* **16**, 527
Hapke, B.: 1990, *Icarus* **88**, 407.
Hovenier, J. W. and de Haan, J. F.: 1985, *Astron. Astrophys.* **146**, 185.
Hovenier, J. W., van de Hulst, H. C., and van der Mee, C. V. M.: 1986, *Astron. Astrophys.* **157**, 301.
Hovenier, J. W. and van der Mee, C. V. M.: 1983, *Astron. Astrophys.* **128**, 1.
Ishimaru, A. and Tsang, I.: 1988, *J. Opt. Soc. Amer. A* **5**, 228.
Ishimaru, A. and Yeh, C. W.: 1984, *J. Opt. Soc. Amer. A* **1**, 359.
Mishchenko, M. I.: 1990, *J. Quant. Spectrosc. Radiat. Tranfer* **43**, 163.
Mishchenko, M. I.: 1991a, *J. Quant. Spectrosc. Radiat. Transfer* **46**, 171.
Mishchenko, M. I.: 1991b, *Phys. Rev. B* **44**, 12597.
Mishchenko, M. I.: 1992a, *J. Opt. Soc. Amer. A*, **9**, 978.

Mishchenko, M. I.: 1992b, *Astrophys. Space Sci.*, in press.
Mishchenko, M. I. and Dlugach, J. M.: 1992a, *Mon. Not. Roy. Astron. Soc.* **254**, Short Communication, 15.
Mishchenko, M. I. and Dlugach, J. M.: 1992b, *Astrophys. Space Sci.*, **189**, 151.
Nieto-Vesperinas, M. and Dainty, J. C. (eds.): 1990, *Scattering in Volumes and Surfaces*, North-Holland, Amsterdam.
Ostro, S.: 1982, in D. Morrison (ed.), *Satellites of Jupiter*, Univ. of Arizona Press, Tucson, p. 213.
Sheng, P. (ed.): 1990, *Scattering and Localization of Classical Waves in Random Media*, World Scientific, Singapore.
Tang, L., Kong, J. A., and Shin, R. T.: 1985, *Theory of Microwave Remote Sensing*, Wiley-Interscience, New York.
van Albada, M. P., van der Mark, M. B., and Lagendijk, A.: 1988, *J. Phys. D* **21**, S28.
van de Hulst, H. C.: 1957, *Light Scattering by Small Particles*, Wiley, New York.
van der Mark, M. B., van Albada, M. P. and Lagendijk, A.: 1988, *Phys. Rev. B* **37**, 3575.
Wolf, P. E., Maret, G., Akkermans, E., and Maynard, R.: 1988, *J. Phys.* (*Paris*) **49**, 63.